Atmos. Chem. Phys. Discuss., 15, 8073–8111, 2015
www.atmos-chem-phys-discuss.net/15/8073/2015/
doi:10.5194/acpd-15-8073-2015

Atmospheric Chemistry and Physics Discussions

Formation of secondary organic aerosol in the Paris pollution plume and its impact on surrounding regions

Q. J. Zhang[1,*], M. Beekmann[1], E. Freney[2], K. Sellegri[2], J. M. Pichon[2], A. Schwarzenboeck[2], A. Colomb[2], T. Bourrianne[3], V. Michoud[1], and A. Borbon[1]

[1]Laboratoire Interuniversitaire des Systèmes Atmosphériques (LISA/IPSL), UMR CNRS 7583, Université Paris Est Créteil (UPEC) and Université Paris Diderot (UPD), France
[2]Laboratoire de Météorologie Physique, Clermont-Ferrand, France
[3]Centre National de Recherches Météorologiques, Météo-France, Toulouse, URA1357, France
[*]now at: ARIA Technologies, Boulogne-Billancourt, France

Received: 19 January 2015 – Accepted: 27 February 2015 – Published: 17 March 2015

Correspondence to: Q. J. Zhang (qzhang@aria.fr)

Published by Copernicus Publications on behalf of the European Geosciences Union.

Abstract

Secondary pollutants such as ozone, secondary inorganic aerosol, and secondary organic aerosol formed in the plume of megacities can affect regional air quality. In the framework of the FP7/EU MEGAPOLI project, an intensive campaign was launched in the Greater Paris Region in July 2009. The major objective was to quantify different sources of organic aerosol (OA) within a megacity and in its plume. In this study, we use airborne measurements aboard the French ATR-42 aircraft to evaluate the regional chemistry-transport model CHIMERE within and downwind the Paris region. Slopes of the plume OA levels vs. O_x ($= O_3 + NO_2$) show secondary OA (SOA) formation normalized with respect to photochemical activity and are used for specific evaluation of the OA scheme in the model. Simulated and observed slopes are in good agreement, when the most realistic "high-NO_x" yields are used in the Volatility-Basis-Set scheme implemented into the model. In addition, these slopes are relatively stable from one day to another, which suggest that they are characteristic for the given megacity plume environment. Since OA within the plume is mainly formed from anthropogenic precursors (VOC and primary OA, POA), this work allows a specific evaluation of anthropogenic SOA and SOA formed from primary semi-volatile and intermediate volatile VOCs (SI-SOA) formation scheme in a model. For specific plumes, this anthropogenic OA build-up can reach about 10 µg m^{-3}. For the average of the month of July 2009, maximum increases occur close to the agglomeration for primary OA are noticed at several tens (for POA) to hundred (for SI-SOA) kilometers of distance from the Paris agglomeration.

1 Introduction

The number of large agglomerations ("megacities") is increasing due to population clustering in urban regions (UN, 2011). Human activities in the megacities cause important negative effects on air quality (Gurjar et al., 2010). Pollutants like ozone and

ACPD
15, 8073–8111, 2015

fine particulate matter ($PM_{2.5}$) have recently been the focus of several studies as a result of concerns for human health, impact on ecosystem and climate (IPCC, 2013). Due to their long life time, they have impacts at both the local and regional level. Therefore, adequate emission control strategies for air quality management need to take into account impacts on different scales.

Photochemical ozone formation is related to precursor molecules: nitrogen oxides (NO_x), and volatile organic carbon species (VOC), emitted mainly from human activities, such as traffic, industrial production, solvent use, in addition to biogenic emissions. In large European agglomerations, a VOC limited chemical regime is in general realized (Beekmann and Vautard, 2010), in which ozone production is directly related to that of VOC precursors. Secondary aerosol formation is induced by formation of condensable or semi-volatile species from precursors like NO_x, SO_2, NH_3 and VOC (Seinfeld and Pandis, 2006). Due to the large number of chemical reactions occurring in different phases, secondary organic aerosol (SOA) formation pathways are still uncertain (e.g. Hallquist et al., 2009), its formation is still difficult to estimate quantitatively (e.g. Hodzic et al., 2010; Zhang et al., 2013), and the contribution of anthropogenic vs. biogenic sources are still under debate (e.g. Hallquist et al., 2009; Beekmann et al., 2014).

Field data provide strong constraints on SOA related processes. In particular, the relation between SOA and O_x (O_3+ NO_2) has been used to express SOA formation as a function of oxidant formation (Herndon et al., 2008; Wood et al., 2010; Hayes et al., 2013; Morino et al., 2014). Indeed, in a "VOC-limited regime" in an urban area, such as Paris, VOC oxidation by OH, ozone or NO_3 is the rate limiting step for both SOA and ozone or O_x production. The ratio or slope of SOA vs. O_x represents the ratio of the photochemical production of SOA to the photochemical production of O_x, both from VOC oxidation, that is, the SOA yield normalized by current photochemical conditions characterized by VOC precursors and oxidant agents availability. It is expected to vary for different VOC species, in particular as a function of their SOA yields, which are for instance large for aromatics and terpenes, while low for alkanes and alkenes (Wood et al., 2010). This is reflected in larger SOA vs. O_x slopes observed

ACPD
15, 8073–8111, 2015

in Mexico City (typically 0.16 $\mu g\,m^{-3}\,ppb^{-1}$), in Los Angeles (0.15 $\mu g\,m^{-3}\,ppb^{-1}$, Hayes et al., 2013) and in Tokyo (0.19 $\mu g\,m^{-3}\,ppb^{-1}$, Morino et al., 2014) than in Houston (typically 0.03 $\mu g\,m^{-3}\,ppb^{-1}$) where petrochemical alkene emissions are large (Wood et al., 2010) (Fig. 1).

The main objective of the MEGAPOLI Paris campaign in summer 2009 was to determine organic aerosol sources in a post-industrial megacity and in its plume. In this work, we apply the regional chemistry transport model (CTM) CHIMERE (Menut et al., 2013) during the MEGAPOLI summer campaign in order to evaluate the model performance against airborne measurements especially for organic aerosol and to assess the impact of Paris agglomeration emissions on OA formation in surrounding regions.

Different configurations of the SOA formation schemes are implemented into CHIMERE, in particular the Volatility-Basis-Set (VBS) approach (Robinson et al., 2007; Donahue et al., 2006; Murphy and Pandis, 2009; Lane et al., 2008a). Based on ground level evaluation with data from the MEGAPOLI summer campaign, Zhang et al. (2013) show a better agreement with OA measurements, when taking into account the volatility of primary organic aerosol (POA), the existence of additional intermediate VOC (IVOC), as well as the chemical aging of the semi-volatile VOC from anthropogenic and biogenic origin. However, SOA was overestimated during long range transport episodes. This result is consistent with previous studies for the Mexico City plume (Dzepina et al., 2011) and for Los Angeles plume (Hayes et al., 2014).

In the framework of the MEGAPOLI project, airborne measurements were performed with the French ATR-42 aircraft operated by the SAFIRE (a CNRS-MétéoFrance–CNES headed unit) in order to document the evolution of pollutants within the Paris agglomeration pollution plume during the MEGAPOLI summer campaign (Freney et al., 2014). The advantage of the airborne measurements over the ground based ones is to follow the evolution of the city plume over time and space up to 200 km downwind of the emissions. Data from these flights will be used to extend the model evaluation performed in Zhang et al. (2013) for urban and suburban sites in the Paris agglomeration to plume conditions. Focus is again to monitor the build-up of secondary organic aerosol within

ACPD
15, 8073–8111, 2015

the plume in relation with tracers of primary emissions, and photochemical activity. In particular, the OA/O_x ratio will be analyzed and used for model evaluation.

For megacities, sources of organic aerosol are still under debate and need to be quantified (e.g. Molina et al., 2010). While in Beekmann et al. (2014), the local vs. advected and the fossil vs. non fossil nature of OA sources within the agglomeration is analyzed, here we focus on additional OA build-up in the agglomeration plume, and on its impact on aerosol concentrations in the surrounding of Paris.

The paper is organized as follows. In Sect. 2, the airborne measurements during the MEGAPOLI summer campaign are described. Model configuration and simulations set-up for the VBS approach to model POA and SOA are introduced in Sect. 3. The evaluation of model performance for plume simulations is presented in Sect. 4, and the impact on regional air quality is described in Sect. 5.

2 Airborne measurement during the MEGAPOLI summer campaign

Flight patterns flown during the MEGAPOLI campaign (Fig. 2) consisted of several transects of the pollution plume at increasing distances from the urban area (Freney et al., 2014). Flight legs perpendicular to the plume time were chosen long enough (50–100 km) to sample rural background conditions at the lateral plume edges. Taking into account the aircraft autonomy of about 3.5 h, this allowed flying four legs across the plume. The maximal distance for a flight was about 200 km from the Paris agglomeration center. The flight level was chosen to lie well inside of the well-developed afternoon convective boundary layer, at about 500–700 m above ground. In addition to measurements inside and outside the Paris plume, each flight included a complete circle around the agglomeration, performed after starting and before landing at the Cergy-Pontoise airport. In this work, we focus only on measurements downwind of Paris to study the pollution production from Paris emissions. The measurements started in the early afternoon in order to sample photo-chemically processed air. Because of a limited number of flight hours, and in line with the principal objective to document the photochemi-

ACPD
15, 8073–8111, 2015

cal production of pollutants, light wind ($< 3\,m\,s^{-1}$) and cloud free weather conditions were privileged. For this study, three flights were chosen on the 16, 21 and 29 July, all of which encountered well pronounced plumes of primary and secondary pollutants. Meteorological conditions for these days were characterized by southerly winds, low wind speed over the agglomeration, elevated temperature and cloudless skies. These conditions favor the accumulation of primary pollutants and photochemical processes leading to the formation of secondary pollutants like O_3 and SOA.

An extensive set of gas phase pollutants and aerosol species and properties were measured on each flight (Freney et al., 2014). For this work, for each flight, a complete measurement set of primary pollutants, BC and NO_x (NO and NO_2), and of secondary pollutants, O_3 and OA, is available and analyzed. Measurement frequencies of all instruments, including the aerosol chemical composition, are rapid enough ($< 40\,s$) to have a relatively good spatial resolution. All measurements during the flights are corrected to temperature (22 °C) and pressure (950 hPa) of the plane (Freney et al., 2014). Thus compared to other values given in this paper and taken at standard conditions, our values are about 5 % lower. Table 1 summarizes the deployed instruments and the measured concentration levels for these pollutants during these flights. Only measurements at a stable flight altitude are used for this study.

The 30 percentile concentrations on the flight legs downwind of Paris represent the background levels of pollutants. For NO_x and BC, they are 1.11, 1.03 and 1.14 ppb, and 0.33, 0.49 and $0.38\,\mu g\,m^{-3}$ on 16, 21 and 29, respectively (Table 1). The rather homogeneous background pollutant levels (Figs. 2 and 3) correspond to the absence of major urban pollution sources south of the Paris agglomeration (rural "Centre" region). The Paris pollution plumes are always clearly identifiable as sharp concentration increases, with continuity on all flight legs at different distances from the agglomeration (Figs. 2 and 3). The plume half-widths are about several tens of kilometers. Maximum plume concentrations of NO_x and BC are 13.5, 7.98 and 12.2 ppb, and 2.00, 2.01 and $2.30\,\mu g\,m^{-3}$, respectively for the three flights (Table 1).

ACPD
15, 8073–8111, 2015

The maximum plume ozone concentrations of are 62.0, 79.0 and 62.4 ppb during these flights, respectively, as compared to the 30th percentile (i.e. background) concentrations of 49.0, 58.0 and 50.0 ppb (Table 1). The largest O_3 values are observed at the flight leg most distant from the agglomeration, allowing for the longest photochemical processing (Fig. 4). For the 16th, the transects across the plume show a double maximum and a relative central minimum due to ozone titration by NO.

The background concentrations of OA are 3.87, 6.47 and 4.13 $\mu g\,m^{-3}$, respectively during these three flights (Table 1, Fig. 5). Maximum plume OA concentrations are 5.97, 12.33 and 7.36 $\mu g\,m^{-3}$, respectively. Thus, additional OA build-up within the plume is about 2 to 6 $\mu g\,m^{-3}$ (see also below in Sect. 4.2). Maximum concentrations appear in the three outer flight legs. OA plumes are wider and less homogeneous than primary pollutant ones, which could be due to a secondary organic aerosol production from additional biogenic sources, in addition to formation from emissions in the Paris agglomeration.

OA vs. O_x ($O_x = O_3 + NO_2$) plots from measurements on these flights are used to study the ratio of the photochemical productivity of OA and O_x build-up in the plume from Paris emissions following an approach first proposed by Herndon et al. (2008). In this study, OA is used instead of SOA, because contrary to SOA, it is directly measured. Among OA factors derived from Positive Matrix Factorization of AMS measurements, LV-OOA (Low volatility oxygenated) and SV-OOA (Semi volatile oxygenated OA) are commonly attributed to SOA (Hallquist et al., 2009). These factors made up for about 70 % of resolved OA factors during MEGAPOLI flights (Freney et al., 2014). HOA (hydrocarbon like OA) make up for the remaining 30 % (and always below 39 %). While this factor is generally attributed to POA, it might partly also correspond to oxidized POA, considered as SOA (Aumont et al., 2012; Cappa and Wilson, 2012). Thus use of OA in this study avoids these attribution problems.

The Pearsons *R* correlation between OA and O_x on the three flights on 16, 21 and 29 is around 0.70 (Table 4, Fig. 6). It indicates a similar ratio of photochemical production of ozone and OA from VOC precursors, though as expected the match between OA and

ACPD
15, 8073–8111, 2015

O_x is not perfect, due to differences in SOA and O_x yields for different VOC precursors. The OA/O_x slopes for these flights are 0.14–0.15 µg m^{-3} ppb^{-1}. This result is close to the one obtained from a previous flight study of urban air mass in Mexico City (0.14–0.15 µg m^{-3} ppb^{-1}, Wood et al., 2010). It is also close to ground-based study, downwind urban emissions from ground-based measurements in Mexico City (median OOA vs. O_x slope of 0.16 µg m^{-3} ppb^{-1}, Wood et al., 2010), in Los Angeles (0.15 µg m^{-3} ppb^{-1}, Hayes et al., 2013) and in Tokyo (0.19 µg m^{-3} ppb^{-1}, Morino et al., 2014).

3 Simulations

3.1 Model configuration

In this work, we used the CHIMERE v2008b version (see http://www.lmd.polytechnique.fr/chimere/) (Vautard al. 2001; Bessagnet et al., 2009; Menut et al., 2013), widely used for operational regional air quality forecast (Honoré et al., 2008; Zhang et al., 2012) and simulations in Europe (e.g. Beekmann and Vautard, 2010; Sciare et al., 2010). With a few exceptions (noted below), the same model configuration as in Zhang et al. (2013) was set-up. Two nested domains are applied: a continental domain covering Europe with a resolution of 0.5° (35–57.5° N, 10.5° W–22.5° E) and a regional domain over Northern France covering all the flight patterns during this campaign with a resolution of 3 km (called MEG3 domain). 8 hybrid-sigma vertical layers are used, with the first layer extending from ground to about 40 m, and a model top at 500 hPa. Tropospheric photochemistry is represented using the reduced MELCHIOR chemical mechanism (Lattuati, 1997; Derognat et al., 2003), including 120 reactions and 44 prognostic gaseous species. For the simulation of the particulate phase, 8 bins of particulate sizes are used in the model with diameters ranging from 0.04 to 10 µm. The thermodynamic equilibrium of the inorganic species (sulfate, nitrate, and ammonium) between the gas and particle phase is interpolated from a tabulation calculated with the ISORROPIA model (Nenes et al., 1998). The evaporation and condensation

ACPD
15, 8073–8111, 2015

processes related to departures from the thermodynamic equilibrium are kinetically controlled. The volatility basis set approach (VBS) is implemented in the model as in Murphy and Pandis (2009) and Lane et al. (2008a). Similar to Zhang et al. (2013), the chemical aging of POA (i), of additional IVOC (ii), of the semi-volatile VOC from both (iii) anthropogenic and (iv) biogenic origin are all taken into account. For the large domain, anthropogenic gas phase emissions are calculated from EMEP annual totals (http://www.ceip.at/emission-data-webdab/), while black carbon (BC) and primary organic aerosol (POA) are prescribed from an emissions inventory prepared by Laboratoire d'Aérologie (Junker and Louisse, 2008). Biogenic emissions are calculated using the MEGAN model data and parameterizations (Guenther et al., 2006). Meteorological fields are simulated with the MM5 mesoscale model (Dudhia, 1993). Boundary conditions are taken from a monthly climatology of the LMDz-INCA2 and LMDz-AERO general circulation model (Hauglustaine et al., 2004).

3.2 Simulation configurations

Here, a brief summary on the two distinct simulation configurations with different emissions and SOA yields in the inner domain is given.

The *VBS-LNOX* simulation in which high SOA yields under low-NO_x conditions are used (the same as the so-called VBS-MPOLI simulation in Zhang et al., 2013), assuming that most of OA is advected to the Paris agglomeration from outside (Petetin et al., 2014a) and probably formed under low-NO_x conditions (Table 2). The emissions inventory on the MEG3 domain is from the emission inventory of the MEGAPOLI project prepared by TNO for both gas-phase and particulate phase in which the refined Paris emissions from Airparif with a resolution of 1 km are integrated (Timmermans et al., 2013).

The VBS–HNOX simulation in which lower SOA yields under high-NO_x conditions (Murphy and Pandis, 2009; Lane et al., 2008,) are used for the MEG3 domain (see Table 2). This is more realistic for SOA formation in the Paris agglomeration and in its plume. All other model settings are equal to the VBS-LNOX configuration.

ACPD
15, 8073–8111, 2015

4 Model evaluation with airborne measurements

In this section, modeling results of NO_x, BC, O_3, and OA are presented and compared to the airborne measurements at the same location and time. Outputs from simulations are interpolated to the exact flight location and time. NO_x and BC are compared as primary urban tracers to indicate the location of the Paris plume in observations and in simulations, respectively. Only the VBS-LNOX simulations are used for BC, NO_x and O_3, because a change of the SOA yields does not affect the simulation of the concentrations of these species. Individual species comparisons are presented in Sect. 4.1 while model observation comparisons of the OA/O_x ratio are presented in Sect. 4.2. For each of the 4 to 5 transects through the pollution plume of a flight, the simulated and observed maximum concentrations are depicted and averaged over all transects of a flight. The same procedure is applied for P30 percentiles over each transect, considered as representative for background conditions outside of the plume.

4.1 Individual species model to observation comparisons

The visual inspection of simulated and observed BC plumes shows that the plume direction is correctly simulated on the 21 and 29, while a difference of about 20° occurs on 16 (Fig. 2). This is still acceptable due to the rather circular structure of the agglomeration. Both in the modeled fields and in observations, most important concentrations appear close to the Paris agglomeration during these three flights.

The modeled maximum BC concentrations are underestimated by −0.7 (−35 %), −1.5 (−74 %) and −1.6 $\mu g\,m^{-3}$ (−70 %) with respect to the measurement, respectively for the 16, 21, and 29. An average underestimation of plume BC measurements by −20 % (over 10 flights during July 2009) was already noticed by Petetin et al. (2014b). It could not be unambiguously attributed to errors in emission inventories, because of uncertainty in measurement and in the choice of the mass specific absorption coefficient (Petetin et al., 2014b). The modeled 30th percentile BC concentrations taken as representative for background are also underestimated by −0.2 (−51 %), −0.3 (−62 %)

ACPD
15, 8073–8111, 2015

and −0.2 µg m^{-3} (−59 %), respectively during these flights (Table 3, Fig. 2). As for BC, the model underestimates NO_x concentrations by −4.3 (−32 %), −5.2 (−65 %) and −7.3 ppb (−60 %) for the maximum concentrations and by −0.6 (−58 %), −0.4 (−41 %) and −0.6 ppb (−52 %) for the background concentrations with respect to the measurement (Table 3). As for BC, the modeled NO_x maximum concentrations are located close to the Paris agglomeration (Table 3).

The modeled O_3 concentrations are slightly overestimated compared to the measured O_3 concentrations, by 7.5 (12 %), 4.3 (5 %) and 8.3 ppb (13 %) for the maximum concentrations, and 4.3 (9 %), 11.3 (20 %) and 3.0 ppb (6 %) for the background concentrations during the three flights, respectively. Note that for O_x, the concentrations can be slightly less overestimated, by respectively 8.5 (13 %), 3.6 (4 %), 8.0 ppb (12 %), for the maximum concentrations, and 3.0 (6 %), 11.0 (19 %) and 1.8 ppb (4 %) for the background concentrations due to the opposite sign in O_3 and NO_x differences with measurements. Similar to the observations, the modeled maximum O_3 levels are located at farthest distances from the agglomeration. The measured OA plume is correlated with the measured BC plume on 16 and 21, while it appears translated to the west for an unknown reason on 29, as is also the ozone plume (Figs. 3–5). On the contrary, in the simulations OA, O_3, BC, and NO_x plumes coincide for all dates, indicating an impact from the Paris emissions. As expected, simulations with the VBS-HNOX configuration show lower plume concentrations than those with the VBS-LNOX configuration, because of lower yields in SOA formation in the inner MEG3 domain. Background simulations are similar for both simulations corresponding to low NO_x yields chosen for both configurations in the larger domain. The maximum concentration of OA simulated with VBS-LNOX is overestimated with respect to the measurement by 1.7 (28 %), 0.4 (3 %) and 1.5 µg m^{-3} (21 %) on 16, 21 and 29, respectively, while it fits well the observations in VBS-HNOX, being slightly underestimated by −0.5 (−8 %), −1 (−8 %) and −0.5 µg m^{-3} (−7 %). These differences are small compared to usually strong OA underestimations in earlier modelling studies (e.g. Volkamer et al., 2006; Sciare et al., 2010 for the Paris region). The modeled OA background concentrations are underestimated

ACPD
15, 8073–8111, 2015

both on 16 and on 29 by VBS-LNOX, by −1.6 (−41 %) and −1.0 µg m^{-3} (−25 %), and VBS-HNOX, by −1.1 (−50 %) and −0.4 µg m^{-3} (−33 %). They are overestimated with both configurations on the 21, by 2.3 (36 %) and 1.9 µg m^{-3} (29 %), respectively. All in all, simulated and observed OA concentrations are rather similar, which is valuable in light of often very large model to observation differences reported in literature (e.g. Sciare et al., 2010 for the Paris region). However, as the primary pollutants and oxidant levels are not quite as nicely predicted by the model compared to OA, this might be the result of compensating errors. In the following, we will investigate the relative contribution of OA to O_x in the Paris plume for a better insight of the results.

4.2 OA plume build-up

First, the plume productions of OA (and of O_x) are derived here from the difference between maximum and background (30th percentile) concentrations over the transects as given in the last section. O_x is preferred here with respect to O_3 since it is not affected by titration with NO. For the three flight days (16, 21 and 29), measured values of OA plume build-up are 2.1, 5.9 and 3.2 µg m^{-3}, while they are 5.4, 4.0 and 5.8 µg m^{-3} in VBS-LNOX and 3.5, 3.0 and 4.1 µg m^{-3} in VBS-HNOX. Thus, irrespectively of the model configuration used, overestimations of plume OA occur on two days (16 and 29), while an underestimation appears on the 21.

The plume O_x production, calculated again from the difference between the maximum concentrations and the background concentrations are 12.9, 21.8 and 12.6 ppb from the measurements and 18.4, 14.4 and 18.8 ppb in the simulations (again for the three flight days respectively). As for OA, we encounter an overestimation of plume O_x for the 16 and 29, and an underestimation for the 21. This suggests that the representation of photochemical conditions might be partially responsible for differences observed for OA, and thus that the given data set could not be used directly for evaluation of the OA scheme in the model.

ACPD
15, 8073–8111, 2015

To overcome these problems, we analyze here OA vs. O_x plots. As explained in the introduction, the slopes of these plots can represent in plume OA build-up, normalized with respect to the availability of VOC precursors and oxidant agents (OH, O_3 and NO_3). This holds under the ideal hypothesis of a constant mix of VOC precursors and oxidant agents for the considered data points of a flight. In Sect. 2, we presented correlations of about 0.7 (R) between OA and O_x measured on the flight legs for a given day. Modeled OA and O_x on these flight legs show even higher correlation of more than 0.95 (Table 4). These good correlations suggest that we are close enough to the "constant mix" hypothesis to make the OA vs. O_x slope a useful metrics. The simulated slopes of OA/O_x are 0.23, 0.29 and 0.26 $\mu g\,m^{-3}\,ppb^{-1}$ with the VBS-LNOX configuration for the three flights on 16, 21 and 29, respectively (Fig. 6). They overestimate the measured slopes of 0.13, 0.14 and 0.15 $\mu g\,m^{-3}\,ppb^{-1}$ by a factor between 1.7 and 2. Note the small variability in the relative differences between flights due to the normalizing method (i.e. plotting OA vs. O_x to normalize with respect to photochemical conditions). This overestimation can now be unambiguously related to the OA scheme: it is likely that the high SOA yields under low-NO_x conditions are incorrect under plume conditions. The corresponding slopes in the VBS-HNOX simulation with lower yields under high NO_x conditions are 0.15, 0.24 and 0.19 $\mu g\,m^{-3}\,ppb^{-1}$, respectively. These slopes show a much lower overestimation of a factor of 1.1, 1.7 and 1.3 for the three days. The measured slopes of OA vs. O_x during the first two flight legs on these days are close to the ones during the last two flight legs. The modeled slopes of OA vs. O_x, 0.12, 0.23 and 0.17 $\mu g\,m^{-3}\,ppb^{-1}$ are close to the measured ones which are 0.12, 0.18 and 0.16 $\mu g\,m^{-3}\,ppb^{-1}$ during the first two flight legs, while the modeled ratios, 0.17, 0.25 and 0.21 $\mu g\,m^{-3}\,ppb^{-1}$ are overestimated by 1.3, 1.9, and 1.3 with respect to the measured ones during the last two flight legs. Thus, the overestimation of slopes occurs especially during the last two flight legs (Figs. 7 and 8). It is related to relatively higher anthropogenic SOA formation due to continuous chemical aging when the flights are farther away from Paris fresh emissions. Such higher slopes during the last two flight legs than during the first two flight legs are not seen for BSOA, probably because these

ACPD
15, 8073–8111, 2015

emissions are more diffuse. Even if some differences are made evident, such a good agreement in OA vs. O_x slopes between simulations and measurements represents a valuable validation of the VBS scheme for the conditions of the Paris plume.

5 Impact of Paris plume on surrounding regions

In this section, we analyse the contribution of OA build-up from emissions in or near the Paris agglomeration to regional OA levels. This analysis is based on simulations with the VBS-HNOX configuration. We will first analyse the individual build-up of OA species for the three flight days (Sect. 5.1), then we will study the time evolution of a pollution plume on the 16 July (Sect. 5.2), and finally, we present average results for July 2009.

5.1 Plume build-up of individual OA species

The slopes of modeled SI-SOA (SOA from oxidation of primary semi-volatile and intermediate volatile VOCs, previously referred as OPOA in Zhang et al. (2013), ASOA (anthropogenic SOA) and BSOA (biogenic SOA) vs. O_x are well correlated, generally with $R > 0.7$ (Table 4). They are used here to analyze the plume production of individual OA species. SI-SOA is formed by functionalization and condensation of evaporated POA and IVOC species (Robinson et al., 2007) which are thought to be constituted by long alkane chains. SI-SOA vs. O_x slopes are 0.04, 0.02, and 0.03 $\mu g\,m^{-3}\,ppb^{-1}$ for the three flights, respectively. They represent 27, 8, and 16 % of the total OA vs. O_x slopes. Thus SI-SOA has only a minor contribution to Paris plume OA formation. The anthropogenic photochemical production of ASOA from aromatics dominates the OA production on 16 and 29, with slopes of 0.10 and 0.09, and of 0.08 $\mu g\,m^{-3}\,ppb^{-1}$ on the 21. Thus, on the 29 and especially on 16, the SOA production is strongly influenced by anthropogenic emissions (by more than 90 %). A major contribution of anthropogenic VOC emissions to OA build-up in the Paris plume during MEGAPOLI flights has also

ACPD
15, 8073–8111, 2015

been found by Freney et al. (2014), from a conjoint analysis by AMS OA measurements, and PTR-MS VOC compounds. These results imply important SOA formation from the Paris agglomeration VOC and to a lesser extent POA and IVOC emissions. On the contrary, BSOA formation dominates the SOA production on 21, with a slope of BSOA vs. O_x of 0.15 $\mu g\,m^{-3}\,ppb^{-1}$, about 63 % of the slope of OA vs. O_x. BSOA formation can both be due to fresh BVOC emissions from mainly isoprene emitting forests north of Paris or from condensation of biogenic SVOC when temperatures decrease in the later afternoon.

5.2 Time evolution of the plume on 16 July

Figure 9 gives a typical picture of the OA species evolution in the Paris plume (at surface). On 16 July at 07:00 UTC, a morning peak of OA is formed inside the Paris agglomeration as a result of POA emissions, low wind speeds, and a low boundary layer height and is transported northeast. It disappears in the later morning (10:00 UTC) due to an increase of the PBL height and stronger winds. In the early afternoon (13:00 UTC), an OA plume is formed at about 50 km from the agglomeration center due to photochemical SOA production. At 16:00 UTC, the plume travels further northeast. Largest OA values occur between 49.5° N and 50° N, about 100 km north of Paris, in agreement with measurements. Major contributors ASOA and SI-SOA add more than 5 and 2 $\mu g\,m^{-3}$ of OA to the plume maximum (Fig. 10). The ASOA and SI-SOA plumes are clearly cut from the Paris agglomeration, (i) because of the time needed for processing of precursor emissions, and (ii) because of the largest accumulation of precursor emissions in the early morning hours when wind speeds over the agglomeration were very low (also seen in the POA peak at the same location). BSOA contributes to the regional background and is little affected by anthropogenic Paris agglomeration emissions (Fig. 10). The highest OA concentrations of about 10 $\mu g\,m^{-3}$ occurs in the evening at 19:00 UTC in northern France (at ~ 150 km distance from the from the agglomeration center) due to continuous photochemical SVOC production and aging,

ACPD
15, 8073–8111, 2015

and due to lower temperatures. At 22:00 UTC, the plume is leaving the MEG3 model domain.

This phenomenon of continuing SOA formation which is detached from the original rush hour emission area due to transport is very similar to that observed for Los Angeles in the CalNex study (Hayes et al., 2013).

5.3 Average July 2009 urban OA contribution to the surroundings of Paris

Here, we analyze the regional scale OA build-up from the Paris emissions for the average of July 2009 from the VBS-HNOX simulation (Figs. 11 and 12). Average OA concentrations around the Paris agglomeration do not show distinctive pollution plumes, but instead a strong W–E gradient near the agglomeration, presumably due to averaging different plume directions, and due to differences in background conditions. OA values also show strong decreasing gradients at about 100 to 150 km in the N–NE of Paris. This behavior can be analyzed by considering specifically the contributions to OA.

Average POA from Paris emissions is only about 0.15 $\mu g\,m^{-3}$ over Paris and the area of enhanced values is extending to E/NE because of the largest climatological frequency of south-westerly to westerly winds in July. The areas of enhancements of POA occur on a length scale of some tenths of kilometers around the agglomeration. ASOA is enhanced within the agglomeration and within the SW and NNE plume, up to 100 to 150 km downwind the agglomeration respectively. The maximum concentrations in these plumes are 0.4 and 0.35 $\mu g\,m^{-3}$, respectively (always for the July 2009 average). In the NNE direction, enhanced values originate from pollution events under SW flow such those studied in this work (see Sect. 5.2). The enhanced values in SW originate from a pronounced pollution plume occurring in the beginning of July, for which no measurements were available. SI-SOA is most enhanced in the NNE direction where its maximum concentration is about 0.35 $\mu g\,m^{-3}$, thus somewhat smaller than the ASOA concentration. It is noted that these increases in ASOA and SI-SOA concentrations are much larger when analyzing individual events than when looking at averages, due

ACPD
15, 8073–8111, 2015

to different plume angles on different days, thus diluting the average fields. The BSOA component does not show distinct plumes, but a continuous NW/W–SE/E gradient, that is the continental character of air masses implies large average BSOA concentrations. BSOA is the strongest contributor to OA over the domain. Its gradient is responsible for the W–E OA gradient noticed earlier, with smaller contributions from the other components.

6 Conclusion

CHIMERE simulations are used to study the secondary pollutant formation in the Paris plume and its impact on the surrounding regions. This study focusses on three photochemically active days for which airborne observations are available. Primary pollutants, such as NO_x and BC, are underestimated in the model. However, ozone is slightly overestimated in the plume and in background. Predicted (and measured) OA is very well correlated with predicted (and measured) O_x. The ratio of the photochemical productivities of SOA and O_x (slope of OA vs. O_x) is well simulated (overestimation of less than 30 %) when low SOA yields are applied on the SOA formation scheme. This is an important result in evaluating the VBS scheme with terrain data. Combined with similar recent results for the Tokyo megacity (Morino et al., 2014), it show the good performance of the VBS scheme in large urban areas or their plumes. When considering the OA to O_x slopes, the day to day variability in model to observation results is much lower than for OA alone. Observed OA vs. O_x slopes of about 0.14 to 0.15 $\mu g\, m^{-3}\, ppb^{-1}$ compare well to those observed in the Mexico City, the Los Angeles and the Tokyo plumes. It is likely that these values remain rather similar for a large range of emission and photochemical conditions. Studies under various conditions (type of emissions, season, photochemical aging ...) would be needed to further substantiate this conclusion. ASOA, formed from oxidation of aromatics, generally dominates the in-plume SOA production during the flight within 100 km from Paris. Background OA concentrations are dominated by BSOA due to long range transport from Southern France.

ACPD
15, 8073–8111, 2015

Predicted maximum OA is found on the flight leg most distant from the agglomeration (at about 150 km), as for observations, indicating secondary anthropogenic SOA formation from Paris emissions over all the distances and during several hours. On a monthly average, OA from Paris emissions contributes to the OA regional build-up at different length scales, from several tenths for POA to several hundreds of kilometers for ASOA and SI-SOA. Clearly, ASOA build-up from precursor emissions in the Paris agglomeration affects atmospheric composition at regional scale. Simulating this build-up has been possible only after an original model evaluation showing good agreement between simulated and observed OA to O_x slopes. These slopes are an interesting parameter to measure the SOA build-up efficiency of a given environment.

Acknowledgements. The research leading to these results has received funding from the European Community's Seventh Framework Programme FP/2007-2011 under grant agreement n° 212520. Support from the French ANR project MEGAPOLI – PARIS (ANR-09-BLAN-0356), from the CNRS-INSU/FEFE via l'ADEME (n° 0962c0018) and the Ile de France/SEPPE are acknowledged. We would like to thank the pilots, the flight crew, and the whole SAFIRE team for operating the ATR-42 aircraft. Q. J. Zhang was supported by Ph.D. grant from French CIFRE (ANRT).

References

Aumont, B., Valorso, R., Mouchel-Vallon, C., Camredon, M., Lee-Taylor, J., and Madronich, S.: Modeling SOA formation from the oxidation of intermediate volatility *n*-alkanes, Atmos. Chem. Phys., 12, 7577–7589, doi:10.5194/acp-12-7577-2012, 2012.

Beekmann, M. and Vautard, R.: A modelling study of photochemical regimes over Europe: robustness and variability, Atmos. Chem. Phys., 10, 10067–10084, doi:10.5194/acp-10-10067-2010, 2010.

Beekmann, M., Prévôt, A. S. H., Drewnick, F., Sciare, J., Pandis, S. N., Denier van der Gon, H. A. C., Crippa, M., Freutel, F., Poulain, L., Ghersi, V., Rodriguez, E., Beirle, S., Zotter, P.,von der Weiden-Reinmüller, S.-L., Bressi, M., Fountoukis, C., Petetin, H., Szidat, S., Schneider, J., Rosso, A., El Haddad, I., Megaritis, A., Zhang, Q. J., Slowik, J. G.,

ACPD
15, 8073–8111, 2015

Moukhtar, S., Kolmonen, P., Stohl, A., Eckhardt, S., Borbon, A., Gros, V., Marchand, N., Jaffrezo, J. L., Schwarzenboeck, A., Colomb, A., Wiedensohler, A., Borrmann, S., Lawrence, M., Baklanov, A., and Baltensperger, U.: Regional emissions control fine particulate matter levels in the Paris megacity, Atmos. Chem. Phys. Discuss., submitted, 2014.

Bessagnet, B., Menut, L., Curci, G., Hodzic, A., Guillaume, B., Liousse, C., Moukhtar, S., Pun, B., Seigneur, C., and Schulz, M.: Regional modeling of carbonaceous aerosols over Europe – focus on secondary organic aerosols, J. Atmos. Chem., 61, 175–202, 2009.

Cappa, C. D. and Wilson, K. R.: Multi-generation gas-phase oxidation, equilibrium partitioning, and the formation and evolution of secondary organic aerosol, Atmos. Chem. Phys., 12, 9505–9528, doi:10.5194/acp-12-9505-2012, 2012.

Derognat, C., Beekmann, M., Baeumle, M., Martin, D., and Schmidt, H.: Effect of biogenic volatile organic compound emissions on tropospheric chemistry during the atmospheric pollution over the Paris Area (ESQUIF) campaign in the Ile-de-France region, J. Geophys. Res., 108, 8560, doi:10.1029/2001JD001421, 2003.

Donahue, N. M., Robinson, A. L., Stanier, C. O., and Pandis, S. N.: Coupled partitioning, dilution, and chemical aging of semivolatile organics, Environ. Sci. Technol., 40, 2635–2643, 2006.

Dudhia, J.: A nonhydrostatic version of the Penn State/NCAR mesoscale model: validation tests and simulation of an Atlantic cyclone and cold front, Mon. Weather Rev., 121, 1493–1513, 1993.

Dzepina, K., Cappa, C. D., Volkamer, R. M., Madronich, S., DeCarlo, P. F., Zaveri, R. A., and Jimenez, J. L.: Modeling the multiday evolution and aging of secondary organic aerosol during MILAGRO 2006, Environ. Sci. Technol., 45, 3496–3503, 2011.

Freney, E. J., Sellegri, K., Canonaco, F., Colomb, A., Borbon, A., Michoud, V., Doussin, J.-F., Crumeyrolle, S., Amarouche, N., Pichon, J.-M., Bourianne, T., Gomes, L., Prevot, A. S. H., Beekmann, M., and Schwarzenböeck, A.: Characterizing the impact of urban emissions on regional aerosol particles: airborne measurements during the MEGAPOLI experiment, Atmos. Chem. Phys., 14, 1397–1412, doi:10.5194/acp-14-1397-2014, 2014.

Guenther, A., Karl, T., Harley, P., Wiedinmyer, C., Palmer, P. I., and Geron, C.: Estimates of global terrestrial isoprene emissions using MEGAN (Model of Emissions of Gases and Aerosols from Nature), Atmos. Chem. Phys., 6, 3181–3210, doi:10.5194/acp-6-3181-2006, 2006.

ACPD
15, 8073–8111, 2015

Gurjar, B. R., Jain, A., Sharma, A., Agarwal, A., Gupta, P.,Nagpure, A. S., and Lelieveld, J.: Human health risksin megacities due to air pollution, Atmos. Environ., 44, 4606–4613, 2010.

Hallquist, M., Wenger, J. C., Baltensperger, U., Rudich, Y., Simpson, D., Claeys, M., Dommen, J., Donahue, N. M., George, C., Goldstein, A. H., Hamilton, J. F., Herrmann, H., Hoffmann, T., Iinuma, Y., Jang, M., Jenkin, M. E., Jimenez, J. L., Kiendler-Scharr, A., Maenhaut, W., McFiggans, G., Mentel, Th. F., Monod, A., Prévôt, A. S. H., Seinfeld, J. H., Surratt, J. D., Szmigielski, R., and Wildt, J.: The formation, properties and impact of secondary organic aerosol: current and emerging issues, Atmos. Chem. Phys., 9, 5155–5236, doi:10.5194/acp-9-5155-2009, 2009.

Hauglustaine, D. A., Hourdin, F., Jourdain, L., Filiberti, M. A., Walters, S., Lamarque, J.-F., and Holland, E. A.: Interactive chemistry in the Laboratoire de Meteorologie. Dynamique general circulation model: description and background tropospheric chemistry evaluation, J. Geophys. Res., 109, D04314, doi:10.1029/2003JD003957, 2004.

Hayes, P. L., Ortega, A. M., Cubison, M. J., Froyd, K. D., Zhao, Y., Cliff, S. S., Hu, W. W., Toohey, D. W., Flynn, J. H., Lefer, B. L., Grossberg, N., Alvarez, S., Rappenglück, B., Taylor, J. W., Allan, J. D., Holloway, J. S., Gilman, J. B., Kuster, W. C., Gouw, J. A., Massoli, P., Zhang, X., Liu, J., Weber, R. J., Corrigan, A. L., Russell, L. M., Isaacman, G., Worton, D. R., Kreisberg, N. M., Goldstein, A. H., Thalman, R., Waxman, E. M., Volkamer, R., Lin, Y. H., Surratt, J. D., Kleindienst, T. E., Offenberg, J. H., Dusanter, S., Griffith, S., Stevens, P. S., Brioude, J., Angevine, W. M., Jimenez, J. L.: Organic aerosol composition and sources in Pasadena, California during the 2010 CalNex campaign, J. Geophys. Res.-Atmos., 118, 9233–9257, doi:10.1002/jgrd.50530, 2013.

Hayes, P. L., Carlton, A. G., Baker, K. R., Ahmadov, R., Washenfelder, R. A., Alvarez, S., Rappenglück, B., Gilman, J. B., Kuster, W. C., de Gouw, J. A., Zotter, P., Prévôt, A. S. H., Szidat, S., Kleindienst, T. E., Offenberg, J. H., and Jimenez, J. L.: Modeling the formation and aging of secondary organic aerosols in Los Angeles during CalNex 2010, Atmos. Chem. Phys. Discuss., 14, 32325–32391, doi:10.5194/acpd-14-32325-2014, 2014.

Herndon, S., Onasch, T., Wood, E. C., Kroll, J. H., Canagaratna, M., Jayne, J., Zavala, M., Knighton, W. B., Mazzoleni, C., Dubey, M. K., Ulbrich, I., Jimenez, J. L., Seila, R., de Gouw, J. A., De Foy, B., Fast, J., Molina, L., Kolb, C. E., and Worsnop, D. R.: The correlation of secondary organic aerosol with odd oxygen in Mexico City, Geophys. Res. Lett., 35, L15804, doi:10.1029/2008GL034058, 2008.

ACPD
15, 8073–8111, 2015

Hodzic, A., Jimenez, J. L., Madronich, S., Canagaratna, M. R., DeCarlo, P. F., Kleinman, L., and Fast, J.: Modeling organic aerosols in a megacity: potential contribution of semi-volatile and intermediate volatility primary organic compounds to secondary organic aerosol formation, Atmos. Chem. Phys., 10, 5491–5514, doi:10.5194/acp-10-5491-2010, 2010.

Honoré, C., Rouil, L., Vautard, R., Beekmann, M., Bessagnet, B., Dufour, A., Elichegaray, C., Flaud, J.-M., Malherbe, L., Meleux, F., Menut, L., Martin, D., Peuch, A., Peuch, V. H., and Poisson, N.: Predictability of European air quality: the assessment of three years of operational forecasts and analyses by the PREV'AIR system, J. Geophys. Res., 113, D04301, doi:10.1029/2007JD008761, 2008.

IPCC: Climate Change: The Physical Science Basis: Summary for Policymakers, IPCC, Cambridge, UK, 2013.

Junker, C. and Liousse, C.: A global emission inventory of carbonaceous aerosol from historic records of fossil fuel and biofuel consumption for the period 1860–1997, Atmos. Chem. Phys., 8, 1195–1207, doi:10.5194/acp-8-1195-2008, 2008.

Lane, T. E., Donahue, N. M., Pandis, S. N.: Simulating secondary organic aerosol formation using the volatility basis-set approach in a chemical transport model, Atmos. Environ., 42, 7439– 7451, 2008.

Lattuati, M.: Contribution à l'étude du bilan de l'ozone troposphérique à l'interface de l'Europe et de l'Atlantique Nord: modélisation lagrangienne et mesures en altitude, Thèse de sciences, Université Paris 6, Paris, France, 1997.

Menut, L., Bessagnet, B., Khvorostyanov, D., Beekmann, M., Blond, N., Colette, A., Coll, I., Curci, G., Foret, G., Hodzic, A., Mailler, S., Meleux, F., Monge, J.-L., Pison, I., Siour, G., Turquety, S., Valari, M., Vautard, R., and Vivanco, M. G.: CHIMERE 2013: a model for regional atmospheric composition modelling, Geosci. Model Dev., 6, 981–1028, doi:10.5194/gmd-6-981-2013, 2013.

Molina, L. T., Madronich, S., Gaffney, J. S., Apel, E., de Foy, B., Fast, J., Ferrare, R., Herndon, S., Jimenez, J. L., Lamb, B., Osornio-Vargas, A. R., Russell, P., Schauer, J. J., Stevens, P. S., Volkamer, R., and Zavala, M.: An overview of the MILAGRO 2006 Campaign: Mexico City emissions and their transport and transformation, Atmos. Chem. Phys., 10, 8697–8760, doi:10.5194/acp-10-8697-2010, 2010.

Morino, Y., Tanabe, K., Sato, K., and Ohara, T.: Secondary organic aerosol model intercomparison based on secondary organic aerosol to odd oxygen ratio in Tokyo, J. Geophys. Res.-Atmos., 119, 13489–13505, doi:10.1002/2014JD021937, 2014.

ACPD
15, 8073–8111, 2015

Murphy, B. N., Pandis, S. N.: Simulating the formation of semivolatile primary and secondary organic aerosol in a regional chemical transport model, Environ. Sci. Technol., 43, 4722–4728, 2009.

Nenes, A., Pilinis, C., and Pandis, S.: ISORROPIA: a new thermodynamic model for inorganic multicomponent atmospheric aerosols, Aquat. Geochem., 4, 123–152, 1998.

Petetin, H., Beekmann, M., Sciare, J., Bressi, M., Rosso, A., Sanchez, O., and Ghersi, V.: A novel model evaluation approach focusing on local and advected contributions to urban $PM_{2.5}$ levels – application to Paris, France, Geosci. Model Dev., 7, 1483–1505, doi:10.5194/gmd-7-1483-2014, 2014a.

Petetin, H., Beekmann, M., Schwarzenboeck, A., Zhang, Q., Michoud, V., Colomb, A., Sciare, J., Crumeyrolle, S., Dupont, J.-C., Morille, Y., Perrussel, O., and Honoré., C.: Evaluating BC and NO_x emission inventories for the Paris region from MEGAPOLI aircraft measurements, in review, Atmos. Chem. Phys. Discuss., 2014b.

Robinson, A. L., Donahue, N. M., Shrivastava, M. K., Weitkamp, E. A., Sage, A. M., Grieshop, A. P., Lane, T. E., Pierce, J. R., and Pandis, S. N.: Rethinking organic aerosols: semivolatile emissions and photochemical aging, Science, 3155816, 1259–1262, 2007.

Sciare, J., d'Argouges, O., Zhang, Q. J., Sarda-Estève, R., Gaimoz, C., Gros, V., Beekmann, M., and Sanchez, O.: Comparison between simulated and observed chemical composition of fine aerosols in Paris (France) during springtime: contribution of regional versus continental emissions, Atmos. Chem. Phys., 10, 11987–12004, doi:10.5194/acp-10-11987-2010, 2010.

Seinfeld, J. H. and Pandis, S. N.: Atmospheric Chemistry and Physics: From Air Pollution to Climate Changes, John Wiley, Hoboken, NJ, 2006.

Timmermans, R. M. A., Denier van der Gon, H. A. C., Kuenen, J. J. P., Segers, A. J., Honoré, C., Perrussel, O., Builtjes, P. J. H., and Schaap, M.: Quantification of the urban air pollution increment and its dependency on the use of down-scaled and bottom-up city emission inventories, Urban Clim., 6, 46–62, 2013.

United Nations: World Urbanization Prospects, the 2011 Revision, available at: http://www.un.org/en/development/desa/population/publications/pdf/urbanization/WUP2011_Report.pdf (last access: 10 March 2015), New York, 2012.

Vautard, R., Beekmann, M., Roux, J., and Gombert, D.: Validation of a hybrid forecasting system for the ozone concentrations over the Paris region, Atmos. Environ., 35, 2449–2461, 2001.

ACPD
15, 8073–8111, 2015

Volkamer, R., Jimenez, J. L., Martini, F. S., Dzepina, K., Zhang, Q., Salcedo, D., Molina, L. T., Worsnop, D. R., and Molina, M. J.: Secondary organic aerosol formation from anthropogenic air pollution: rapid and higher than expected, Geophys. Res. Lett., 33, L17811, doi:10.1029/2006GL026899, 2006.

Wood, E. C., Canagaratna, M. R., Herndon, S. C., Onasch, T. B., Kolb, C. E., Worsnop, D. R., Kroll, J. H., Knighton, W. B., Seila, R., Zavala, M., Molina, L. T., DeCarlo, P. F., Jimenez, J. L., Weinheimer, A. J., Knapp, D. J., Jobson, B. T., Stutz, J., Kuster, W. C., and Williams, E. J.: Investigation of the correlation between odd oxygen and secondary organic aerosol in Mexico City and Houston, Atmos. Chem. Phys., 10, 8947–8968, doi:10.5194/acp-10-8947-2010, 2010.

Zhang, Q. J., Laurent, B., Velay-Lasry, F., Ngo, R., Derognat, C., Marticorena, B., Albergel, A.: An air quality forecasting system in Beijing – application to the study of dust storm events in China in May 2008, J. Environ. Sci., 24, 102–111, doi:10.1016/S1001-0742(11)60733-X, 2012.

Zhang, Q. J., Beekmann, M., Drewnick, F., Freutel, F., Schneider, J., Crippa, M., Prevot, A. S. H., Baltensperger, U., Poulain, L., Wiedensohler, A., Sciare, J., Gros, V., Borbon, A., Colomb, A., Michoud, V., Doussin, J.-F., Denier van der Gon, H. A. C., Haeffelin, M., Dupont, J.-C., Siour, G., Petetin, H., Bessagnet, B., Pandis, S. N., Hodzic, A., Sanchez, O., Honoré, C., and Perrussel, O.: Formation of organic aerosol in the Paris region during the MEGAPOLI summer campaign: evaluation of the volatility-basis-set approach within the CHIMERE model, Atmos. Chem. Phys., 13, 5767–5790, doi:10.5194/acp-13-5767-2013, 2013.

ACPD
15, 8073–8111, 2015

Table 1. Airborne chemical instruments deployed, the measurements by these instruments are used to discuss general findings during the campaign (Freney et al., 2014) and evaluate the model simulations.

Pollutant	Instrument	Time resolution	Unit	Statistics	Concentration		
					16	21	29
NO_x	MONA[1]	30 s	ppb	Max.	13.5	7.98	12.2
				30th percentile	1.11	1.03	1.14
O_3	UV analyser[2]	30 s	ppb	Max.	62.0	79.0	62.4
				30th percentile	49.0	58.0	50.0
BC	PSAP[3]	1 s	$\mu g\,m^{-3}$	Max.	2.00	2.01	2.30
				30th percentile	0.33	0.49	0.38
OA	C-ToF-AMS[4]	30 s	$\mu g\,m^{-3}$	Max.	5.97	12.3	7.36
				30th percentile	3.87	6.47	4.13

[1] Measurement Of Nitrogen on Aircraft developed at by the Laboratoire Interuniversitaire des Systems Atmospheres (LISA).
[2] Thermal-environmental instruments O_3 UV analyser.
[3] Radiance research® Particulate Soot Absorption Photometer.
[4] Aerodyne Compact Time-of-flight Aerosol Mass Spectrometer.

ACPD
15, 8073–8111, 2015

Table 2. Secondary organic aerosol (SOA) mass yields used in this work. These yields are for surrogate VOC species with saturation concentrations of 1, 10, 100 and 1000 $\mu g\,m^{-3}$ at 298 K (Murphy and Pandis, 2009).

VOCs	VBS-LNOX with low-NO_x condition				VBS-HNOX with high-NO_x condition			
	1	10	100	1000	1	10	100	1000
ALK4[1]	0	0.075	0	0	0	0.0375	0	0
ALK5[2]	0	0.3	0	0	0	0.15	0	0
OLE1[3]	0.0045	0.009	0.06	0.225	0.0008	0.0045	0.0375	0.15
OLE2[4]	0.0225	0.0435	0.129	0.375	0.003	0.0255	0.0825	0.27
ARO1[5]	0.075	0.225	0.375	0.525	0.003	0.165	0.3	0.435
ARO2[6]	0.075	0.3	0.375	0.525	0.0015	0.195	0.3	0.435
TERP[7]	0.1073	0.0918	0.3587	0.6075	0.012	0.1215	0.201	0.507
ISOP[8]	0.009	0.03	0.015	0	0.0003	0.0225	0.015	0

[1] n-pentane, n-hexane, Branched C5-C6 Alkanes, Cyclopetane, Trimethyl Butane, Trimethyl Pentane, Isopropyl alcool, n-Propyl Alcool.
[2] C7-C22 n-Alkanes, C6-C16 Cycloalkanes, branched/Unspeciated C8-C18 Alkanes.
[3] Propene, C4-C15 terminal Alkanes.
[4] Isobutene, C4-C15 Internal Alkenes, C6-C15 Cyclic or di-olefins, Styrenes.
[5] Toluene, benzene, Ethyl benzene, C9-C13 Monosubstituted Benzenes.
[6] Xylenes, Ethyl Toluenes, Dimethyl and Trimethyl Benzenes, Ethylbezenes, naphthalene, C8-C13 Di-, Tri-, Tetra-, Penta-, Hexa-substituted Benzenes, Unspeciated C10-C12 Aromatics.
[7] α-pinene and sabinene, β-pinene and δ3-carene, limonene, ocimene and myrcene.
[8] Isoprene.

ACPD
15, 8073–8111, 2015

Table 3. Model statistics from VBS-LNOX (and VBS-HNOX for OA as well).

Statistics	Unit	Statistics	Concentration		
			16 July	21 July	29 July
NO_x	ppb	Max.	9.18	2.82	4.92
		30th percentile	0.47	0.61	0.55
BC	$\mu g\,m^{-3}$	Max.	1.3	0.52	0.69
		30th percentile	0.16	0.18	0.16
O_3	ppb	Max.	69.5	83.3	70.7
		30th percentile	53.3	69.3	53
O_x	ppb	Max.	72.1	84.2	72.2
		30th percentile	53.7	69.8	53.4
OA (VBS-LNOX)	$\mu g\,m^{-3}$	Max.	7.66	12.74	8.87
		30th percentile	2.28	8.77	3.09
OA (VBS-HNOX)	$\mu g\,m^{-3}$	Max.	5.48	11.31	6.88
		30th percentile	1.95	8.35	2.85

ACPD
15, 8073–8111, 2015

Table 4. Correlation coefficients of OA/O_x, SI-SOA/O_x, $ASOA/O_x$ and $BSOA/O_x$ for the flights on 16, 21 and 29 July from the measurements and simulations VBS-LNOX and VBS-HNOX.

Data	Date	OA/O_x	$OPOA/O_x$	$ASOA/O_x$	$BSOA/O_x$
AMS	16	0.70			
	21	0.71			
	29	0.72			
VBS-LNOX	16	0.96	0.91	0.96	0.57
	21	0.95	0.77	0.85	0.90
	29	0.98	0.79	0.93	0.84
VBS-HNOX	16	0.95	0.90	0.96	0.45
	21	0.95	0.77	0.92	0.88
	29	0.98	0.78	0.95	0.80

ACPD
15, 8073–8111, 2015

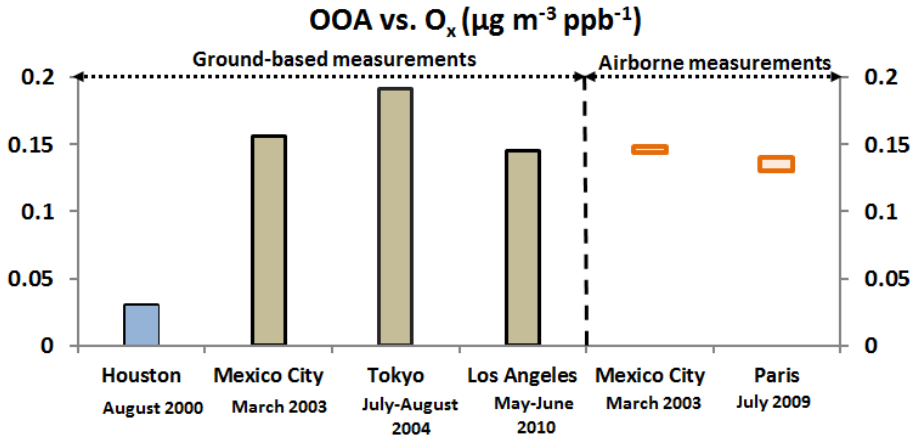

Figure 1. Ratios of OOA vs. O_x from studies in Mexico City, Houston, Los Angeles, Tokyo and Paris. Ratios for Houston, Los Angeles and Tokyo are derived from ground-based measurements during typically one month and located in the metropolitan area. For Houston, the ratio during influences from a combination of urban and petrochemical emissions, typically 0.03 µg m^{-3} ppb^{-1} (Wood et al., 2010), is presented. Ratios for Paris and Mexico City are derived from three and two individual flights, respectively, performed at about 100 to 150 km downwind from the agglomeration.

ACPD
15, 8073–8111, 2015

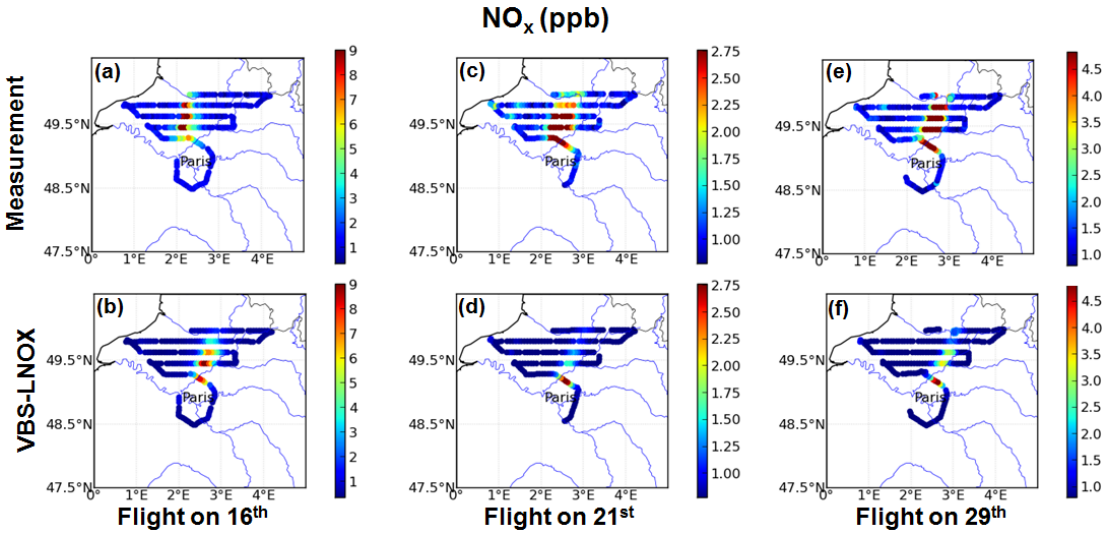

Figure 2. Comparison of measured **(a)**, **(c)**, **(e)** and modeled NO_x from VBS-LNOX **(b)**, **(d)**, **(f)** during the flights on 16, 21 and 29, respectively.

ACPD
15, 8073–8111, 2015

Formation of SOA in the Paris pollution plume and its impact on surrounding regions

Q. J. Zhang et al.

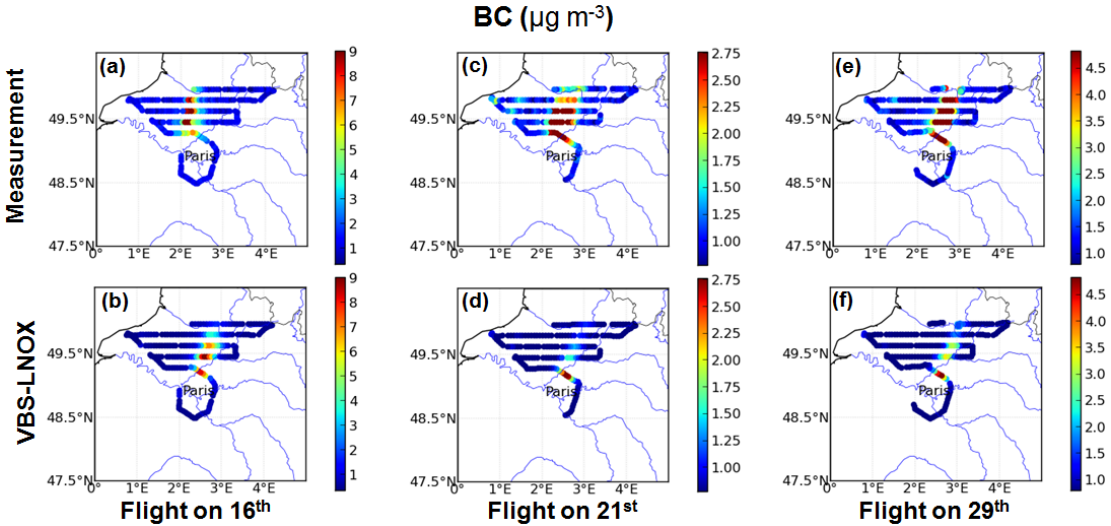

Figure 3. Comparison of measured **(a)**, **(c)**, **(e)** and modeled BC from VBS-LNOX **(b)**, **(d)**, **(f)** during the flights on 16, 21 and 29, respectively.

ACPD
15, 8073–8111, 2015

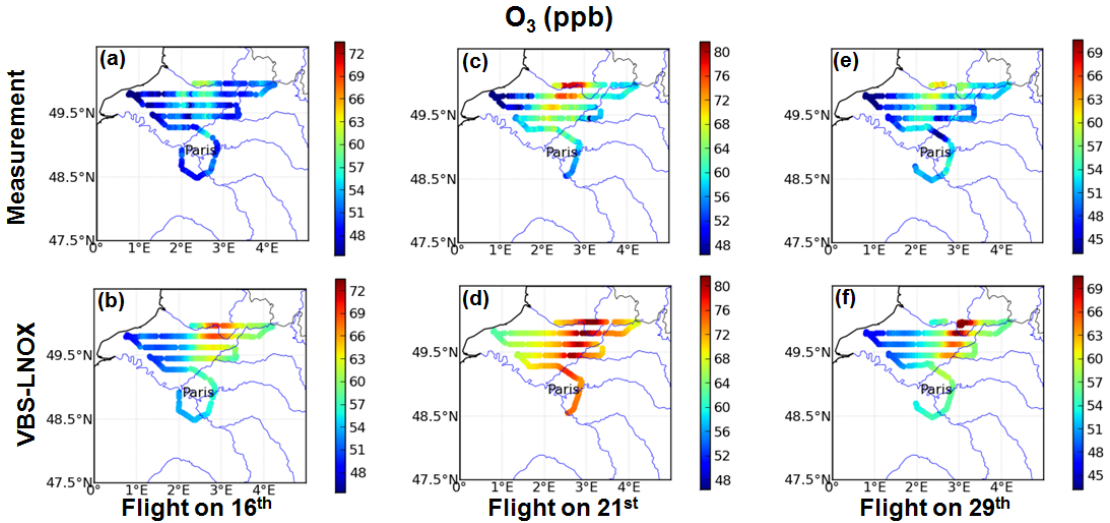

Figure 4. Comparison of measured **(a)**, **(c)**, **(e)** and modeled O_3 from VBS-LNOX **(b)**, **(d)**, **(f)** during the flights on 16, 21 and 29, respectively.

ACPD
15, 8073–8111, 2015

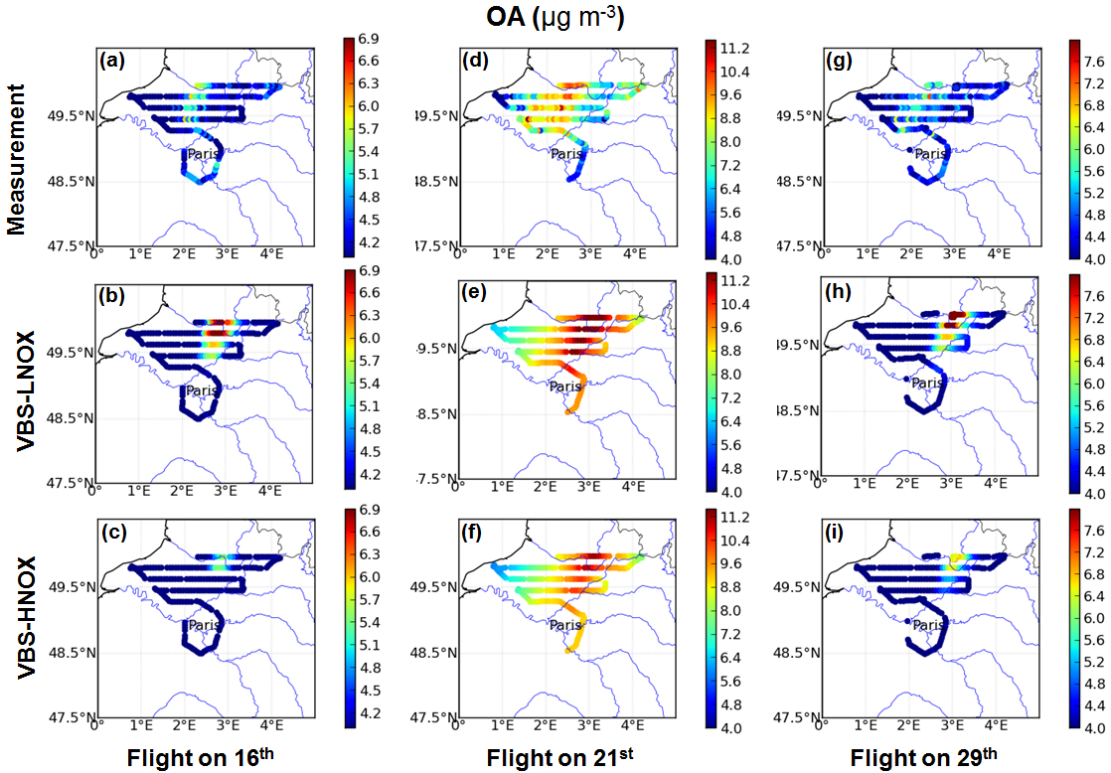

Figure 5. Comparison of measured **(a)**, **(d)**, **(g)** and modeled OA from VBS-LNOX **(b)**, **(e)**, **(h)** and VBS-HNOX **(c)**, **(f)**, **(i)** during the flights on 16, 21 and 29, respectively.

ACPD
15, 8073–8111, 2015

Formation of SOA in the Paris pollution plume and its impact on surrounding regions

Q. J. Zhang et al.

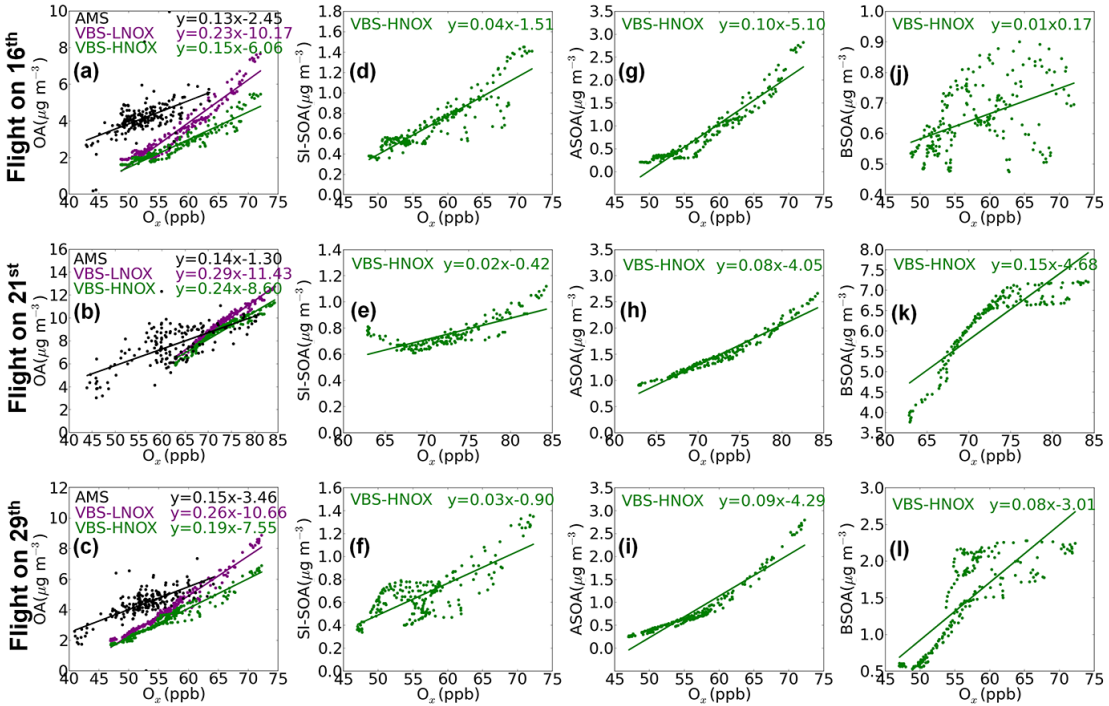

Figure 6. OA vs. O_x **(a–c)**, SI-SOA vs. O_x **(d–f)**, ASOA vs. O_x **(g–i)** and BSOA **(j–l)** vs. O_x during the flights on 16, 21 and 29, respectively. For OA vs. O_x **(a–c)**, results from the measurement, VBS-LNOX and VBS-HNOX are presented. For others, only results from VBS-HNOX are presented.

ACPD
15, 8073–8111, 2015

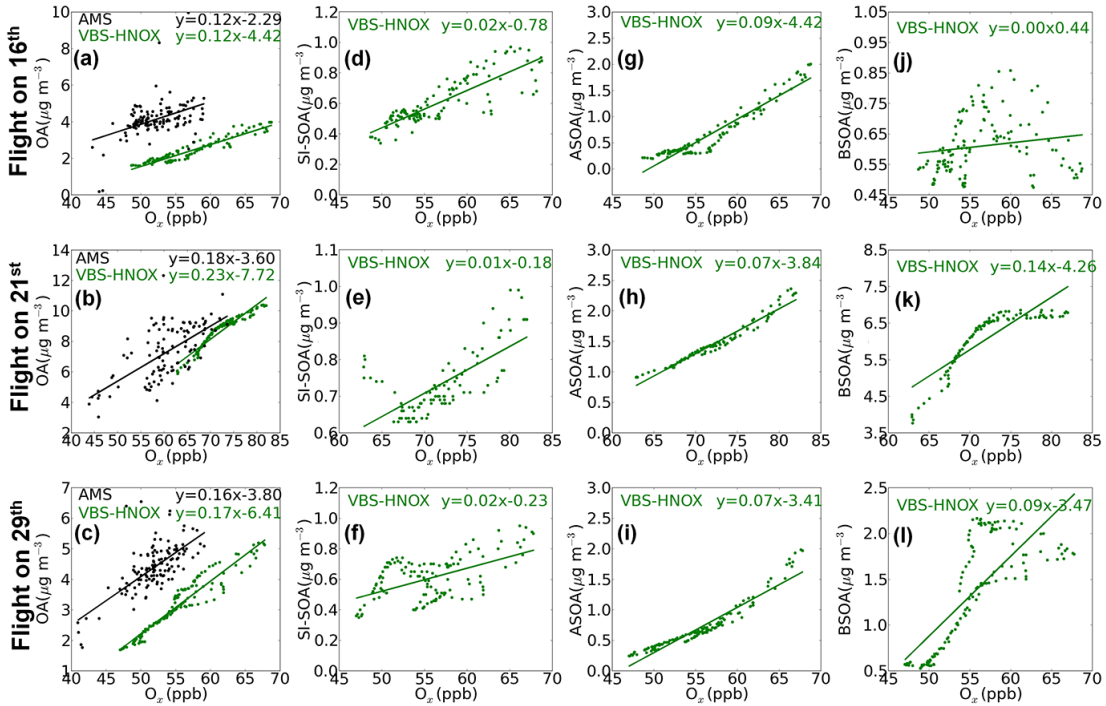

Figure 7. OA vs. O_x **(a–c)**, SI-SOA vs. O_x **(d–f)**, ASOA vs. O_x **(g–i)** and BSOA **(j–l)** vs. O_x during the first two flight legs on 16, 21 and 29, respectively. For OA vs. O_x **(a–c)**, results from the measurement, VBS-LNOX and VBS-HNOX are presented. For others, only results from VBS-HNOX are presented.

ACPD
15, 8073–8111, 2015

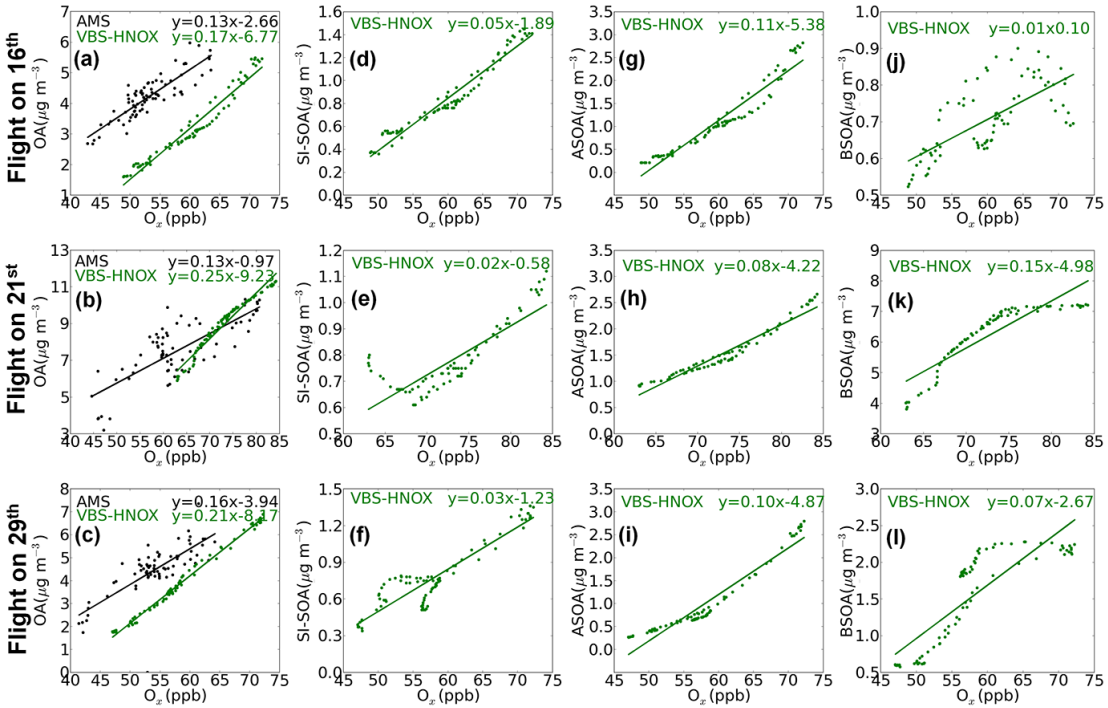

Figure 8. OA vs. O_x **(a–c)**, SI-SOA vs. O_x **(d–f)**, ASOA vs. O_x **(g–i)** and BSOA **(j–l)** vs. O_x during the last two flight legs on 16, 21 and 29, respectively. For OA vs. O_x **(a–c)**, results from the measurement, VBS-LNOX and VBS-HNOX are presented. For others, only results from VBS-HNOX are presented.

ACPD
15, 8073–8111, 2015

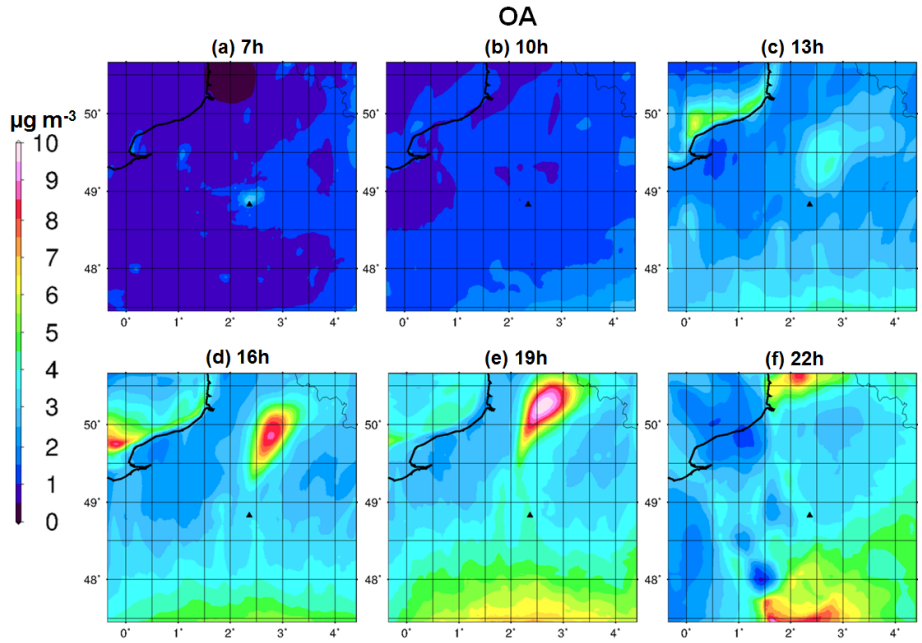

Figure 9. Urban OA (PM_{10} fraction) plume ($\mu g\,m^{-3}$) evolution on 16 July from VBS-HNOX, the triangle represents the location of Paris, illustrated by 6 panels (from **a** to **f** corresponding to 07:00 LT (UTC +2) to 22:00 LT (UTC +2) with a time step of three hours.

ACPD
15, 8073–8111, 2015

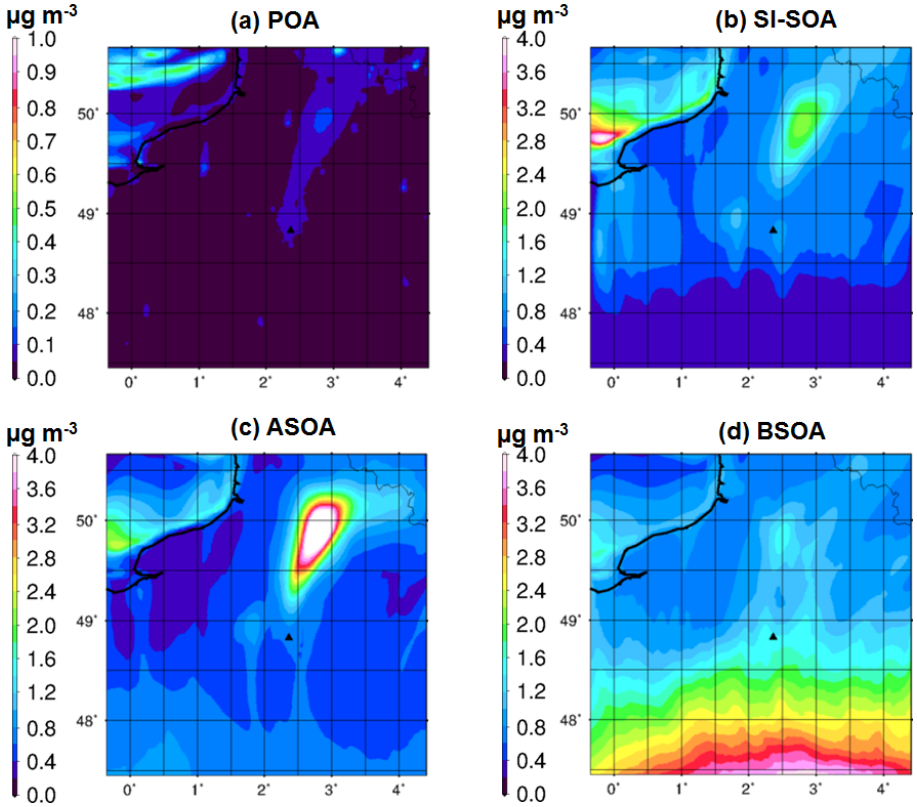

Figure 10. Urban POA **(a)**, SI-SOA **(b)**, ASOA **(c)** and BSOA **(d)** (in PM_{10}) plume ($\mu g\,m^{-3}$) from VBS-HNOX of 16 July, the triangle represents the location of Paris.

ACPD
15, 8073–8111, 2015

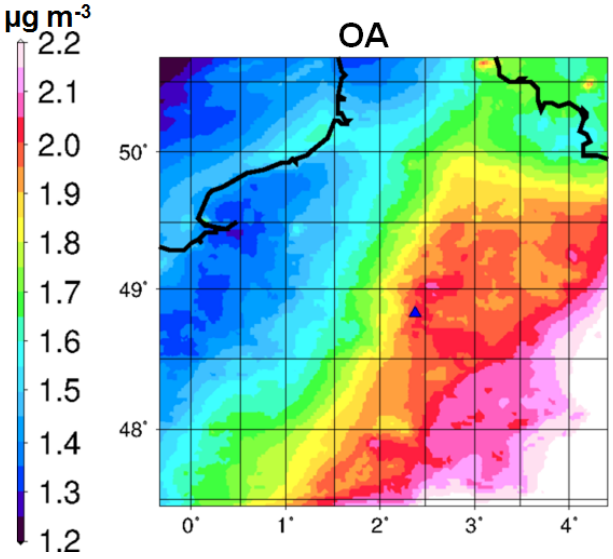

Figure 11. Modeled monthly mean OA concentration in PM_{10} from VBS-HNOX which represents the influence of Paris emissions on OA levels, the triangle represents the location of Paris.

ACPD
15, 8073–8111, 2015

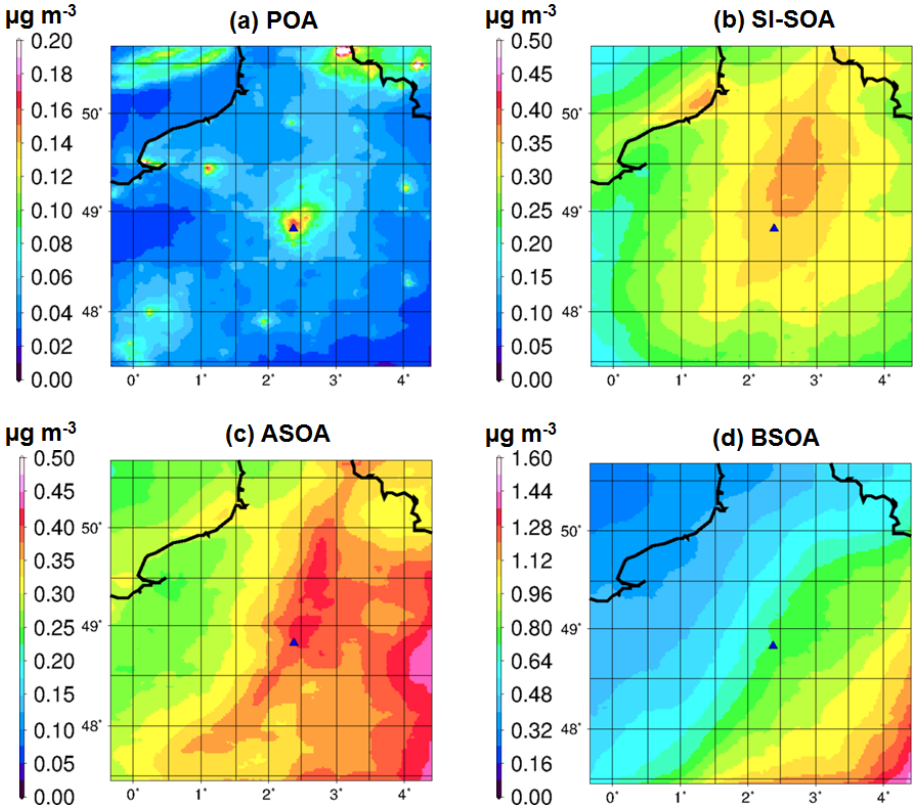

Figure 12. Modeled monthly mean POA **(a)**, SI-SOA **(b)**, ASOA **(c)** and BSOA **(d)** concentration in PM_{10} ($\mu g\,m^{-3}$) from VBS-HNOX which represents the influence of Paris emissions on OA levels, the triangle represents the location of Paris.

ACPD
15, 8073–8111, 2015